Document Version
Final published version

Citation (APA)
Beijnen, L. F. E., Huiskes, M. D., Neto, A., & Sberna, P. (2025). Reflection TDS-THz Characterization and Drude Modelling of N-Type Doped C-Si from Room Temperature to 475 K. In *Proceedings of the 2025 55th European Microwave Conference (EuMC)* (pp. 286-289). (2025 55th European Microwave Conference, EuMC 2025). IEEE. https://doi.org/10.23919/EuMC65286.2025.11235165

Proceedings of the 55th European Microwave Conference

Reflection TDS-THz characterization and Drude modelling of n-type doped c-Si from room temperature to 475 K

Laurens F.E. Beijnen, Martijn D. Huiskes, Andrea Neto, Paolo Sberna

Department of Microelectronics, Delft University of Technology, The Netherlands
p.m.sberna@tudelft.nl

***Abstract* — The mm and sub-mm wave propagation and absorption in n-type c-Si are investigated as a function of temperature by time-domain reflectivity measurements. The temperature range spans from 300 K to 475 K and the complex electric resistivity, extracted from the reflectivity spectra, shows the same free electrons mobility degradation with temperature as observed with previous dc conductivity measurements. The Drude theory of free charge carriers, based on the conduction electron concentration and effective scattering time, well fit the experimental data from 200 GHz to 1 THz. The dependence of the scattering time with respect to the doping concentration and sample temperature is consistent with the empirical unified model for the electron dc mobility, which is widely used in c-Si passive components and device simulations.**

***Keywords* — Time-domain, Reflectivity, THz, Silicon, Drude.**

I. INTRODUCTION

Nowadays, mm and sub-mm wave sensing and communication technologies make an extensive use of crystalline Silicon (c-Si) lenses, absorbers and waveguides [1][2][3] due to its extremely reliable control of material synthesis, machining and hybrid integration of these components with state-of-the-art radiofrequency (RF) microchips [4]. Modelling of the way c-Si microscopic properties affect its electro-magnetic response above 30 GHz, hence, has been an intense activity of the RF engineering research in the last decades. Grischkowsky and co-workers have been one of the first researchers to investigate the propagation and absorption of mm and sub-mm waves into cSi [5][6][7]. Their works employed time-domain (TD) techniques and demonstrated that free charge carriers RF response in doped c-Si is a paradigmatic manifestation of the Drude theory [8]. However, their measurements have been limited to samples at room temperature and below (e.g. 80 K). On the other hand, there is a temperature range, between 300 K and 500 K, where specific free charge carriers scattering mechanisms, enhanced by heating up Si, are characterized solely by dc conductivity and Hall measurements (the most relevant experimental works are reported in [9] and [10]). This temperature interval is of interest for Si-based RF (multi)chip modules and integrated systems dealing with a significant heat power generation.

In this work we extend the studies in [7] to the mm and sub-mm wave TD reflectivity of n-type doped c-Si from 300 K to 475 K. The Drude theory of free conduction electrons, involving their volume concentration N and effective scattering time τ, is then successfully employed to model the temperature-dependent reflection coefficient spectra $\Gamma(T,\omega)$ and related constitutive quantities, such as the effective relative electric permittivity $\varepsilon_{rr,eff}(T,\omega) + j\varepsilon_{ri,eff}(T,\omega)$ and resistivity $\rho_r(T,\omega) + j\rho_i(T,\omega)$. The Drude theory parameters N and τ we have obtained are consistent with the unified model for the temperature dependence of dc electron mobility in [10] thus expanding its applicability to c-Si high frequency response.

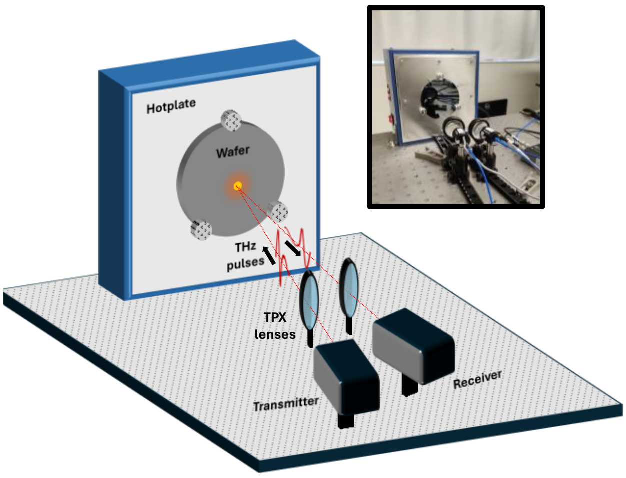

Fig. 1. Representation of the reflection TD spectroscopy setup. The top-right insert shows a picture of setup.

Table 1. Silicon Samples Overview

Sample	ρ_{4pp} $\Omega \cdot cm$	Thickness (μm)	Note
VLRS	0.04	286	Single wafer
LRS	0.4	610	2 bonded wafers
MRS	2	6300	12 stacked wafers
HRS	30	15000	5 stacked wafers

II. SAMPLES AND EXPERIMENTAL SETUP

The characterized samples are presented in Table 1. For all the four samples, the material is doped with Phosphorous. Each sample consists in a single wafer (VLRS) or a stack of intimately bonded (no usage or glue or presence of air gap) wafers of almost uniform doping level. The stacking procedure for the samples with the low and medium resistivity (LRS and MRS) allows to outreach the critical thickness, above which almost all the radiation transmitted inside the material is absorbed without re-emerging after multiple internal reflections. In this way the measured spectra of the reflectivity, effective relative permittivity and complex resistivity show negligible multi-reflection oscillation, rendering the fitting easier and the modelling more accurate. For the sample with the highest resistivity (HRS), it was not practical to work with the critical thickness and the stacking up to a total of 1.5 cm only alleviated the presence of these oscillations to a level for which the data analysis is still manageable. The resistivity of every c-Si wafer has been first measured, at room temperature, by the four-point-probe technique. Then, from the unified electrons mobility versus doping model in [9], we extracted the dc room temperature scattering time τ_{dc} (RT) and the electron concentration N_{dc} (RT) . The dc scattering time for higher temperatures τ_{dc} (T) have been, on the other hand, from [10]. The TD reflectivity measurements have been performed using the setup depicted in Fig. 1. The transmitter, receiver, THz polymeric lenses and the optical delay unit (not shown) are part of the TERA K15 system from Menlo systems [11]. Both the transmitter and the receiver are photoconductive antennas, respectively pumped an gated by the same fiber-coupled fs laser. The delay between the pumping and gating pulses is managed by the optical delay unit. The samples are firmly anchored to a digital hotplate facing the transmitter and the receiver, which have been arranged to have a quasi-orthogonal (< 15°) THz beam incidence and reflection. The hotplate temperature has been set at different values between 300 K and 475 K. The sample top and bottom surface temperatures has been measured with a leaf-head thermo-couple. Top and bottom temperatures occurred to be the same within 5 K, indicating an almost uniform heating of the samples.

In order to calculate the sample reflectivity, for every set temperature, the radiation spectra reflected by its surface has been compared to the reference spectra reflected, at the same temperature, by a perfect reflector, i.e. whose coefficient $\Gamma(T,\ \omega)$ equals -1. For this goal, the back surface of every sample has been coated with a sputtered Al film and its reflected radiation spectra has been acquired simply by flipping the sample. Comparing the sample and reference THz reflected spectra at the same temperature, allows to any mechanical displacement of the sample due to the thermal expansion to almost cancel out. In this way the phase error on the sample reflectivity has been minimized and eventually removed during the subsequent data fitting procedure.

III. RESULTS AND DISCUSSION

The TD measurements of the reflected THz pulse gives the electric field wave form $E(t)$, whose spectrum $E(f)$ is directly obtained by its Fourier transform. Fig. 2 shows the room temperature $E_{Si}(t)$ and $E_{Al}(t)$ reflected respectively by the VLRS sample and by its Al-coated backside. The insert reports the same pulse viewed on a wider time scale. The dominant single-cycle signal of $E_{Si}(t)$, between 38 and 40 ps, is the first reflection from the sample top surface. No subsequent peaks related to the multiple internal reflections re-emerging from the top surface are visible. This condition occurs as a consequence of the complete absorption of the transmitted radiation.

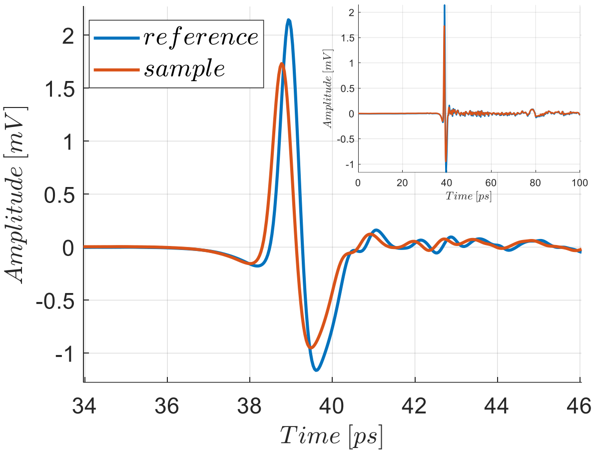

Fig. 2. TD THz pulses reflected by the VLRS sample surface (red curve) and by its reference Al-coated backside surface (blue curve), when both are at $T = 300\,K$.

Fig. 3 shows VLRS sample $E_{Si}(f)$ (dashed curves) and $E_{Al}(f)$ (solid curves), first kept at room temperature (blue curves) and then heated at 475 K (red curves).

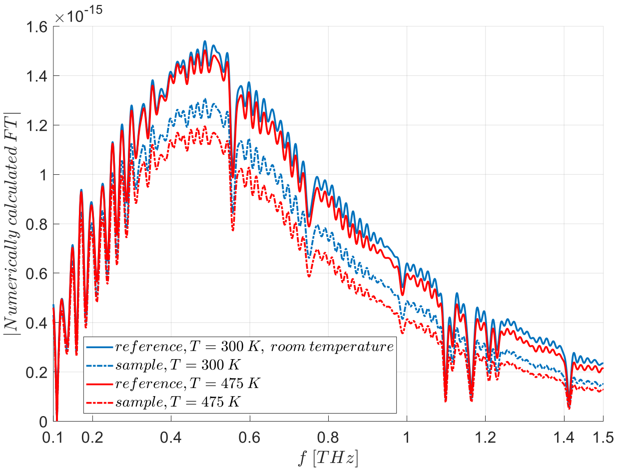

Fig. 3. FT of the TD pulses reflected by the VLRS surface (dashed curves) and by the reference Al-coated backside surface (solid curves). The blue curves correspond to samples and reference kept at $T = 300K$, while the red curves correspond to samples and reference kept at $T = 475K$.

The frequency interval where the level of the S/N is acceptable for our data analysis ranges between 0.2 THz and

1 THz. These boundaries are intrinsic for the TERA K15 setup. Both spectra $E_{Si}(f)$ and $E_{Al}(f)$shows rapid and small-amplitude oscillations all over the frequency range. They are not thus ascribed to the specific sample properties, yet to the non-ideal behaviour of the quasi optical path linking the transmitter to the receiver. Moreover, the presence of water vapour dispersed in air generates the absorption peaks at around 0.56, 0.75, 1.10, 1.11, 1.16, 1.21, 1.23 and 1.41 THz [12]. It is evident that the VLRS $E_{Si}(f)$, is always significantly lower than the reference spectra, and further decrease for higher temperatures. Similar observations have been made for the samples LRS, MRS and HRS.

The sample reflection coefficient Γ_{Si} , at temperatures ranging from $T = 300\,K$ to $T = 475\,K$, has been calculated from:

$$\Gamma_{Si}(f,T) = -\frac{E_{Si}(f,T)}{E_{Al}(f,T)} \tag{1}$$

From the amplitude and phase of the complex-valued reflection coefficient given in (1), one can extract the sample effective relative permittivity:

$$\varepsilon_{r,eff} = \varepsilon_{rr,eff} + j\varepsilon_{ri,eff} = \left(\frac{1-\Gamma_{Si}}{1+\Gamma_{Si}}\right)^2, \tag{2}$$

In the frequency range investigated in this work the contribution to the dispersion of the relative permittivity, at any temperature, comes only from the free charge carriers:

$$\varepsilon_{r,eff}(\omega) = \varepsilon_{r,\infty} - j\frac{\sigma(\omega)}{\omega\cdot\varepsilon_0}, \tag{3}$$

where ω is the frequency, in radians, $\varepsilon_{r,\infty} = 11.8$ is the Si dielectric constant and $\sigma(\omega)$ is the complex conductivity. The complex resistivity $\rho(\omega)$, defined as $\frac{1}{\sigma(\omega)}$, is linked to the fundamental c-Si microscopic quantities by the Drude's theory of free charge carriers [2][8]. According to this model the real and imaginary parts of the resistivity are given by:

$$\rho_r = \frac{m^*}{e^2}\cdot\frac{1}{N\cdot\tau} \tag{4}$$

$$\rho_i(\omega) = \rho_r\omega\tau = \frac{m^*}{e^2}\cdot\frac{\omega}{N}. \tag{5}$$

In these equations, e is the elementary charge, $m^* = 0.26\cdot m_0$ is the electron effective mass in the Si lattice, m_0 is the electron mass in free space, N is the conduction electrons volume concentration and τ, their effective scattering time. Here, the simplest version of Drude theory has been employed, where τ is, to a first approximation, independent of the electrons energy within the conduction band. For the levels of doping of our samples and for the investigated temperatures, the concentration of free holes can always be neglected, while the electrons concentration is independent from temperature and equal to the doping concentration.

The experimental resistivity data, obtained from solving (3) for $\sigma(\omega)$, have been fitted using (4) and (5). The initial guess for the fitting parameters N and τ are the respective dc values $N_{dc}(RT)$ from [9] and $\tau_{dc}(T)$ from [10]. A third fitting parameter is the phase error of the sample reflectivity calculated from the Drude $\rho(\omega)$ solving backwards the equations from (3) to (1). As mentioned in section II, this error is small and generated by the tiny relative displacement of the sample surface coordinate with respect to the reference Al surface when flipped and kept at the same temperature. The best fit value for the phase error is given by the best matching between the Drude calculated reflectivity and the experimental one, given by (1).

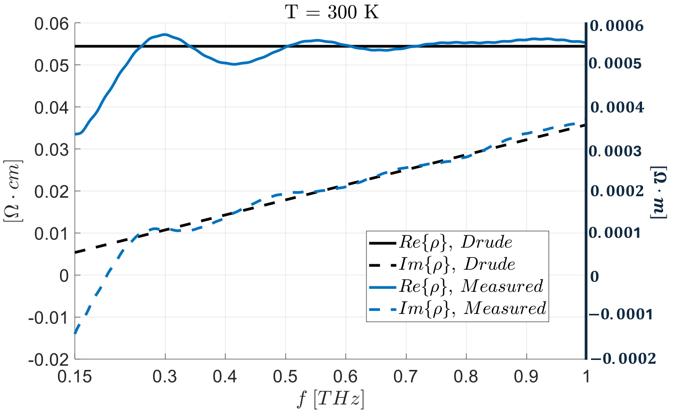

Fig. 4. Real (solid lines) and imaginary (dashed lines) parts of the resistivity of the VLRS sample at $T = 300\,K$.

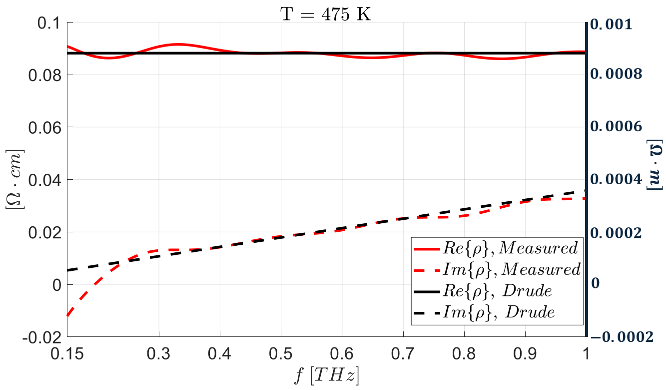

Fig. 5. Real (solid lines) and imaginary (dashed lines) parts of the resistivity of the VLRS sample at $T = 475K$.

Fig.4 and Fig. 5 shows the measured and Drude best fit resistivities, for the VLRS sample at $T = 300\,K$ and at $T = 475\,K$ respectively. The agreement between the Drude theory and the measured curves is excellent within the usable TERA K15 setup frequency range, 0.2 THz – 1 THz. Similar results have been obtained for the rest of the samples, LRS, MRS and HRS. A slightly more complex, yet fundamentally equivalent, data analysis and fitting due to the residual internal multiple reflections was necessary for HRS.

The N and τ resulting from the Drude fitting for all the samples at room temperature are reported in Table 2, together with the respective dc values derived from the 4PP measurements and interrogating [9] and [10].

Table 2. Silicon Drude's Parameters at T = 300 K

Sample	ρ_{4pp} $\Omega \cdot cm$	N_{dc} $[el/m^3]$	τ_{dc} $[s]$	N $[el/m^3]$	τ $[s]$
VLRS	0.04	$4\ 10^{23}$	$0.66\ 10^{-13}$	$1.62\ 10^{23}$	$1.05\ 10^{-13}$
LRS	0.4	$1.33\ 10^{22}$	$1.75\ 10^{-13}$	$0.8\ 10^{22}$	$2.6\ 10^{-13}$
MRS	2	$2.26\ 10^{21}$	$2.04\ 10^{-13}$	$1.61\ 10^{21}$	$3\ 10^{-13}$
HRS	30	$1.42\ 10^{20}$	$2.16\ 10^{-13}$	$0.9\ 10^{20}$	$2\ 10^{-13}$

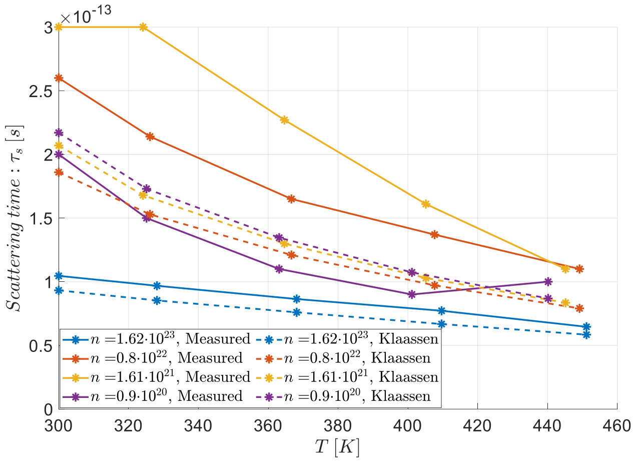

Fig. 6. Scattering time versus temperature for all sample considered in the present work. The measured curves are the solid ones. The dashed curves indicate the scattering time according to the Klaassen for the same doping n.

IV. CONCLUSION

The mm and sub-mm wave propagation and absorption properties of n-type doped c-Si samples have been investigated by TD THz reflection measurements, over the temperature range from 300 K to 475 K. These results, to our knowledge, show for the first time the high frequency response of heated c-Si, which is a material widely used in passive RF components and active devices in RF systems on (multi)chips. The studied temperature range is of great interest for RF modules affected by a significant production of heat. Moreover, the accurate measurement of the THz c-Si reflection coefficient spectrum as a function of temperature puts the basis for a rigorous calculation of c-Si absorptivity (defined as $1 - |\Gamma_{Si}(f,T)|^2$), a quantity of fundamental importance in the theory of radiometry.

This work also demonstrated how the Drude theory of free charge carriers well model the high frequency response of heated c-Si, complementing the pioneering research of Grischkowsky and co-workers [5], [6] and [7], which were limited to room and cryogenic temperatures. As clearly shown in Fig. 6, the conduction electrons effective scattering time obtained from the fitting of our experimental TD data, show a dependence on temperature in accordance with the unified model for mobility discussed in [10], which was based on dc conductivity measurements. This important result shows that the basic features of the currently known microscopic mechanisms, leading to the emergence of an effective scattering time, keeps his validity not only in dc but also in high frequency response. Nevertheless, a small deviation from the scattering curves reported in [10] appears also in Fig. 6. We believe that this fact probably highlights some microscopic details in the scattering modelling which manifest differently depending in which regime, dc or RF, c-Si is studied. Further explanations will be discussed during the conference presentation.

ACKNOWLEDGMENT

The authors thank Dr. Juan Bueno for his support and advise with the TERA K15 setup. The authors thank also Mr. Maarten Haine from DEMO TU Delft for fabricating the wafers support system on the hotplate.

REFERENCES

[1] M. A. Campo, K. Holc, A. Leuther, R. Weber, S. Bruni and N. Llombart, "H-band Silicon Lens Antenna with Quartz Leaky-Wave Feeder and Novel Chip Interconnect," 2020 45th International Conference on Infrared, Millimeter, and Terahertz Waves (IRMMW-THz), Buffalo, NY, USA, 2020, pp. 1-1, doi: 10.1109/IRMMW-THz46771.2020.9370689.

[2] R. M. van Schelven, A. F. Bernardis, P. Sberna and A. Neto, "Drude Dispersion in the Transmission Line Modeling of Bulk Absorbers at Sub-mm Wave Frequencies: A tool for absorber optimization," in IEEE Antennas and Propagation Magazine, vol. 64, no. 1, pp. 50-60, Feb. 2022, doi: 10.1109/MAP.2021.3073092.

[3] T. Reck et al., "A Silicon Micromachined Eight-Pixel Transceiver Array for Submillimeter-Wave Radar," in IEEE Transactions on Terahertz Science and Technology, vol. 5, no. 2, pp. 197-206, March 2015, doi: 10.1109/TTHZ.2015.2397274.

[4] G. Chattopadhyay, T. Reck, C. Jung-Kubiak, M. Alonso-delPino, C. Lee, "Interconnect and packaging technologies for terahertz communication systems", 2017 11th European Conference on Antennas and Propagation (EUCAP), Paris, France, 2017, doi: 10.23919/EuCAP.2017.7928794.

[5] M. van Exter and D. Grischkowsky, "Carrier dynamics of electrons and holes in moderately doped silicon", in Phys. Rev. B, vol. 41, no. 17, pp. 12140-12149, Jun. 1990, doi: 10.1103/PhysRevB.41.12140.

[6] J. Dai, J. Zhang, W. Zhang, and D. Grischkowsky, "Terahertz time-domain spectroscopy characterization of the far-infrared absorption and index of refraction of high-resistivity, float-zone silicon," in J. Opt. Soc. Am. B, vol. 21, no. 7, pp. 1379-1386, Jul. 2004, doi: 10.1364/josab.21.001379.

[7] T. Jeon and D. Grischkowsky, "Characterization of optically dense, doped semiconductors by reflection THz time domain spectroscopy", in Appl. Phys. Lett., vol. 72, no. 23, pp. 3032-3034, Jun. 1998, doi: 10.1063/1.121531.

[8] P. Drude, "Zur Elektronentheorie der Metalle", in Annalen der Physik, vol. 306, no. 3, pp. 566-613, Feb. 1900, doi: 10.1002/andp.19003060312.

[9] D. B. M. Klaassen, "A unified mobility model for device simulation—I. Model equations and concentration dependence," in Solid-State Electronics, vol. 35, no. 7, pp. 953–959, Jul. 1992, doi: 10.1016/0038-1101(92)90325-7.

[10] D. B. M. Klaassen, "A unified mobility model for device simulation—II. Temperature dependence of carrier mobility and lifetime", in Solid-State Electronics, vol. 35, no. 7, pp. 961-967, Jul. 1992, doi: 10.1016/0038-1101(92)90326-8.

[11] Menlo Systems (9 Dic. 2019). Menlo Tera K15 D-EN 2019-12. [PDF]. Available: https://www.menlosystems.com/assets/datasheets/THz-Time-Domain-Solutions/MENLO_TERA_K15_D-EN_2019-12_3w.pdf.

[12] Y.-C. Kim, K.-B. Kim, D.-S. Yee, M.-W. Yi, J.-W. Ahn, "High-speed high-resolution Terahertz time-domain spectrometer", in Korean Journal of Optics and Photonics, vol. 19, no. 5, pp. 370-375, Oct 2008, doi: 10.3807/HKH.2008.19.5.370.